JOURNAL OF GUIDANCE, CONTROL, AND DYNAMICS
Vol. 25, No. 4, July–August 2002

Spacecraft Motion About Slowly Rotating Asteroids

W. Hu and D. J. Scheeres
University of Michigan, Ann Arbor, Michigan 48109-2140

Spacecraft motion about an arbitrary second-degree and second-order gravity field is investigated. We assume that the gravity field is in uniform rotation about an axis of its maximum moment of inertia and that it rotates slowly as compared to the spacecraft orbit period. We derive the averaged Lagrange planetary equations for this system and use them, in conjunction with the Jacobi integral, to give a complete description of orbital motion. We show that, under the averaging assumptions, the problem is completely integrable and can be reduced to quadratures. For the case of no rotation, these quadratures can be expressed in terms of elliptic functions and integrals. For this problem, the orbit plane will experience nutation in addition to the precession that is found for orbital motion about an oblate body. It is possible for the orbit plane to be trapped in a 1:1 resonance with the rotating body, the plane essentially being dragged by the rotating asteroid. As the asteroid rotation rate is increased, this resonant motion disappears for rotation rates greater than a specific value. Finally, we validate our analysis with numerical integrations of cases of interest, showing that the averaging assumptions apply and give a correct prediction of motion in this system. These results are applicable to understanding spacecraft and particle motion about slowly rotating asteroids.

I. Introduction

THIS paper studies the orbital motion of a spacecraft about slowly rotating asteroids. The asteroid gravity field is represented by the second-degree and second-order gravity coefficients C_{20} and C_{22}. The asteroid itself is assumed to be uniformly rotating about the axis of its major moment of inertia. When the asteroid is slowly rotating, we can apply averaging techniques to the Lagrange planetary equations to derive a simplified set of equations that describe a spacecraft's orbit. Also, because this is a uniformly rotating gravity field, the Jacobi integral that is traditionally used for restricted three-body problems is defined for this problem.[1] Using the Jacobi integral in conjunction with the averaged equations, we can show that the problem can be reduced to quadratures, that is, the problem is integrable. This is an extension of the results that show that the averaged problem is integrable in terms of elliptic, hyperbolic, and trigonometric functions if the central body does not rotate.[2] By proper interpretation of the Jacobi integral, we can derive a complete description of the motion of a spacecraft in this problem. For a slowly rotating asteroid, the orbital plane of the spacecraft will either be captured in a stable, 1:1 resonance with the rotating body, or it will circulate with respect to the rotating body. As the rotation rate of the asteroid is increased, the stable 1:1 resonance is driven to higher inclinations until it disappears at a critical value of the asteroid's rotation period.

Orbital motion about an oblate planet (or gravity field with J_2 term only) has been studied extensively, starting in the early 1960s (Refs. 3–6). Most studies that have included the equatorial ellipticity of the central body, that is, the C_{22} gravity term, have made the assumption that this ellipticity is small, as is appropriate for planets in the solar system.[7–9] Our current problem is a significant departure, however, in that it considers values of the C_{22} gravity coefficient that are significantly larger than those found for all solar system planets, making this analysis applicable to asteroids and comets that can have large values of equatorial ellipticity. As has been shown,

Weiduo Hu is a Ph.D. Candidate in the Department of Aerospace Engineering at the University of Michigan. He got his Bachelor degree from Beijing University of Aeronautics and Astronautics. Before he came to the United States, he worked as a senior engineer in Beijing Institute of Control Engineering, dealing with satellite control system design and simulation. His thesis studies spacecraft motion around irregular, rotating asteroids.

Daniel J. Scheeres is currently an Assistant Professor of Aerospace Engineering at the University of Michigan. He received a Ph.D. degree in aerospace engineering from the University of Michigan in 1992. He was a member of the technical staff at the Jet Propulsion Laboratory, California Institute of Technology, from 1992 to 1997 and an Assistant Professor of Aerospace Engineering at Iowa State University from 1997 to 1999 and joined the Aerospace Engineering Department of the University of Michigan in 1999. Current topics of research interest include spacecraft dynamics and navigation in unstable orbital environments, spacecraft formation dynamics and control, and space missions to asteroids and comets.

Received 17 May 2001; revision received 9 January 2002; accepted for publication 9 January 2002.

the basic nature of orbit dynamics about distended, rotating bodies has fundamental differences as compared to orbit dynamics about slightly elliptic bodies.[1] Orbits about asteroids with a relatively rapid rotation rate can experience large, sometimes chaotic changes in orbit energy and angular momentum over short periods of time.[10,11] For resonant orbits about the Earth, rapid changes in semimajor axis have been noted,[9] but the change in semimajor axis is relatively small because the C_{22} of the Earth is small. In contrast, for nonrotating asteroids, all orbital motion is regular and integrable in the averaged case.[2] Of course, averaged systems are integrable in general. (See, for example, the problem of third-body perturbations.[12])

The current paper investigates how orbital dynamics are modified when the central body rotates slowly. There are a significant number of asteroids that fall into this classification.[13,14] Some of these asteroids, such as Toutatis, are potential mission targets.[15] Thus, in addition to being an orbital problem of theoretical interest, this analysis is also of practical interest for future missions.

To give a physically motivated example of what we mean by slow rotation, assume the mean radius of an asteroid is R_A, that its density lies in the range $1 < \rho < 4$, and that a spacecraft orbiting it in a circular orbit has radius r_S. Then the gravity parameter is $\mu = (\frac{4}{3})\pi\rho G R_A^3$, where G is the universal gravity constant, the mean motion of the spacecraft is $n = \sqrt{(\mu/r_S^3)}$, and the period of the spacecraft is

$$T_{S/C} = \frac{2\pi}{n} = \frac{2\pi}{\sqrt{\left(\frac{4}{3}\right)\pi\rho G(R_A/r_S)^3}} \tag{1}$$

For close asteroid orbits, $r_S \approx R_A$. If we choose $\rho = 2.5$, then $T_{S/C} \approx 2$ h. If an asteroid rotation period T is more than 20 h, then we can regard this asteroid as slowly rotating because $T \gg T_S$. About 10% of the asteroids in the solar system fall into this category.[13] Actually, the Earth can also be considered to be slowly rotating for low-altitude orbits, but its C_{22} is very small, and the phenomenon we describe here is not evident. However, Mars's C_{22} is 34 times larger than the Earth's, and so the secular motion for a close Mars orbit could be more significant.

II. Perturbation Model

A. Gravity Field Definitions

For our basic model, we assume an attracting body with gravitational parameter μ and a second-degree and second-order gravity field. We assume that the body-fixed coordinate axes are aligned along the body's principal moments of inertia in such a way that the x axis lies along the moment of minimum inertia, the y axis along the moment of intermediate inertia, and the z axis along the moment of maximum inertia. With this orientation, the second-degree and second-order gravity field can be specified by the two coefficients $C_{20} \le 0$ and $C_{22} \ge 0$. Finally, we assume that the asteroid is in uniform rotation about its maximum moment of inertia (the z axis) with a rotation rate ω_T and a corresponding rotation period $T = 2\pi/\omega_T$.

The gravitational force potential of the second-degree and second-order field in the body-fixed frame is given as[7]

$$U_{20+22} = (\mu/r^3)\left[C_{20}\left(1 - \left(\tfrac{3}{2}\right)\cos^2\delta\right) + 3C_{22}\cos^2\delta\cos 2\lambda\right] \tag{2}$$

where r is the radius of the particle measured from the center of the body, δ is the particle declination measured from the x–y plane, and λ is the particle longitude in the body-fixed frame, measured counterclockwise from the x axis. See Figs. 1 and 2 for the geometry of the problem. The angles δ and λ can be specified in terms of orbital elements:

$$\sin\delta = \sin i \sin u \tag{3}$$

$$\tan\lambda = \frac{\sin\Omega_R\cos u + \cos\Omega_R\sin u\cos i}{\cos\Omega_R\cos u - \sin\Omega_R\sin u\cos i} \tag{4}$$

$$u = \omega + f \tag{5}$$

$$\Omega_R = \Omega - \omega_T t \tag{6}$$

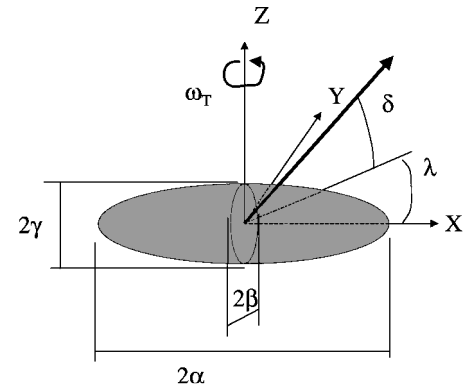

Fig. 1 Position geometry of a spacecraft in the body-fixed space about an asteroid.

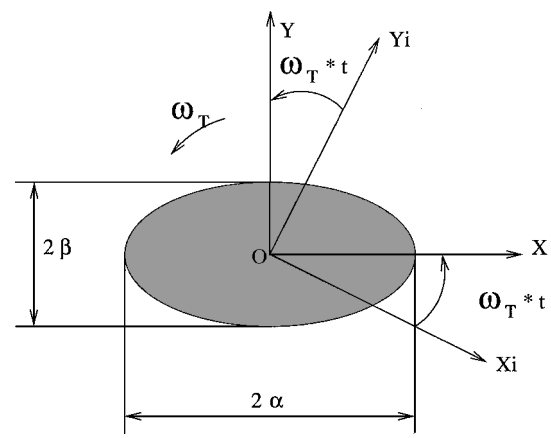

Fig. 2 Plane geometry of the inertial $X_i - O - Y_i$ and the body-fixed $X - O - Y$ coordinates.

where i is the inclination, ω is the argument of periapsis, f is the true anomaly, Ω_R is the longitude of the ascending node in the body-fixed frame, and Ω is the longitude of ascending node in the inertial frame. We note that the time does not explicitly appear in the force potential, indicating that a Jacobi integral will be defined for our system.

B. Asteroid Assumptions

By representing the second-degree and second-order gravity field by the two coefficients C_{20} and C_{22}, we implicitly assume a principal axis coordinate frame. For definiteness, we will specify the frame so that $C_{20} \le 0$ and $C_{22} \ge 0$, implying that the principal moments of inertia are ordered as $I_{xx} \le I_{yy} \le I_{zz}$ with axes x, y, and z (Fig. 1). The relations between the gravity coefficients and the principal moments of inertial of the body (normalized by the body mass) are

$$C_{20} = -\left(\tfrac{1}{2}\right)(2I_{zz} - I_{xx} - I_{yy}) \tag{7}$$

$$C_{22} = \left(\tfrac{1}{4}\right)(I_{yy} - I_{xx}) \tag{8}$$

Then the parameter σ can be defined as

$$\sigma = \frac{I_{yy} - I_{xx}}{I_{zz} - I_{xx}} = -\frac{4C_{22}}{C_{20} - 2C_{22}} \tag{9}$$

where $0 \le \sigma \le 1$ for any mass distribution. A value of $\sigma = 0$ denotes a body with rotational symmetry about the z axis($I_{yy} = I_{xx}$), and a value of $\sigma = 1$ denotes a body with rotational symmetry about the x axis($I_{yy} = I_{zz}$). This parameter will be introduced into the gravitational potential once averaging is performed. The gravity coefficients in terms of this parameter are

$$C_{20} = -\left(\tfrac{1}{2}\right)(I_{zz} - I_{xx})(2 - \sigma) \tag{10}$$

$$C_{22} = \left(\tfrac{1}{4}\right)(I_{zz} - I_{xx})\sigma \tag{11}$$

III. Equations of Motion

A. Full Equations of Motion

The motion of a spacecraft in our system is defined as the solution to the equations of motion:

$$\ddot{x} - 2\omega_T \dot{y} = \omega_T^2 x - \frac{\mu x}{r^3} + \frac{\partial U_{20+22}}{\partial x} \tag{12}$$

$$\ddot{y} + 2\omega_T \dot{x} = \omega_T^2 y - \frac{\mu y}{r^3} + \frac{\partial U_{20+22}}{\partial y} \tag{13}$$

$$\ddot{z} = -\frac{\mu z}{r^3} + \frac{\partial U_{20+22}}{\partial z} \tag{14}$$

These equations are defined in the body-fixed coordinate frame and, thus, include the effect of coriolis and centripetal accelerations. More complete discussions of these equations as applied to motions about an asteroid have been reported.[1]

Because the force potential is time invariant in this formulation, a Jacobi integral exists for this problem:

$$J = \left(\tfrac{1}{2}\right)(\dot{x}^2 + \dot{y}^2 + \dot{z}^2) - \left(\tfrac{1}{2}\right)\omega_T^2(x^2 + y^2) - U_{20+22} - \mu/r \tag{15}$$

$$= -\mu/(2a) - \omega_T\sqrt{\mu a(1-e^2)}\cos i - U_{20+22} \tag{16}$$

where a is the osculating semimajor axis of the orbit, e is the osculating eccentricity, and i is the osculating inclination. This relation is conserved for all solutions to the equations of motion.

B. Averaged Perturbation Function

This paper studies the slowly rotating problem, which means that over one spacecraft orbit period, all of the elements, including Ω_R, can be regarded as constant, as most averaging theories require. This assumption implies that the mean motion of the spacecraft is much faster than the central body rotation rate, or $n = \sqrt{(\mu/a^3)} \gg \omega_T$. When these rates become close to each other, resonant phenomenon will invalidate our basic assumptions.

To formulate an analytical approach to our problem, we average the perturbing potential over the mean anomaly M, specifically computing

$$\bar{U}_{20+22} = \frac{1}{2\pi}\int_0^{2\pi} U_{20+22}\,\mathrm{d}M \tag{17}$$

to find

$$\bar{U}_{20+22} = \left[\mu/2\bar{a}^3(1-\bar{e}^2)^{\frac{3}{2}}\right]\left[C_{20}\left(\tfrac{3}{2}\sin^2\bar{i} - 1\right) + 3C_{22}\sin^2\bar{i}\cos 2\bar{\Omega}_R\right] \tag{18}$$

where the overbars indicate that the orbital elements are now mean orbit elements. At this point, it is useful to introduce our parameter σ, changing the form of the potential to

$$\bar{U}_{20+22} = \frac{-\mu(I_{zz} - I_{xx})}{4\bar{a}^3(1-\bar{e}^2)^{\frac{3}{2}}}\left[\sigma - 2 + 3\sin^2\bar{i}\left(1 - \sigma\cos^2\bar{\Omega}_R\right)\right] \tag{19}$$

C. Averaged Lagrange Equations

In the following, we will drop the overbar notation, implicitly assuming that all orbit elements referenced from this point on, unless otherwise defined, are mean (or averaged) orbital elements. Then, substituting the averaged potential into the Lagrange planetary equations yields[6]

$$\frac{\mathrm{d}a}{\mathrm{d}t} = 0 \tag{20}$$

$$\frac{\mathrm{d}e}{\mathrm{d}t} = 0 \tag{21}$$

$$\frac{\mathrm{d}i}{\mathrm{d}t} = \frac{1}{2}B\sigma\sin i\,\sin 2\Omega_R \tag{22}$$

$$\frac{\mathrm{d}\Omega_R}{\mathrm{d}t} = -B\cos i\left(1 - \sigma\cos^2\Omega_R\right) - \omega_T \tag{23}$$

$$\frac{\mathrm{d}\omega}{\mathrm{d}t} = -\frac{B}{2}\left[\sigma - 4 + 2\sigma\cos^2\Omega_R + 5\sin^2 i\left(1 - \sigma\cos^2\Omega_R\right)\right] \tag{24}$$

$$\frac{\mathrm{d}M}{\mathrm{d}t} = n - \frac{B}{2}\sqrt{1-e^2}\left[\sigma - 2 + 3\sin^2 i\left(1 - \sigma\cos^2\Omega_R\right)\right] \tag{25}$$

where

$$B = 3\mu^{\frac{1}{2}}(I_{zz} - I_{xx})\Big/\left[2a^{\frac{7}{2}}(1-e^2)^2\right] = (3n/2p^2)(I_{zz} - I_{xx}) \tag{26}$$

and semilatus rectum $p = a(1-e^2)$. We note that the semimajor axis and eccentricity are conserved on average, thus implying that orbital energy and angular momentum will be conserved on average. Also, the equations for inclination i and node Ω_R are coupled with each other, whereas the argument of periapsis does not appear in any of the right-hand sides of Eqs. (22–25).

In some situations, the longitude of periapsis will be needed, defined here as $\varpi_\pm = \omega \pm \Omega_R$, the "-" branch is used when $i > 90$ deg:

$$\dot{\varpi}_\pm = (B/2)\left[2 - \sigma - (3 \pm 5\cos i)(1 \mp \cos i) \times\left(1 - \sigma\cos^2\Omega_R\right)\right] \mp \omega_T \tag{27}$$

where the term containing Ω_R will disappear whenever $i = 0$ and 180 deg, whenever it is not defined. Thus, for motion in the equatorial plane ($i = 0$ and 180 deg) the longitude of periapsis will have a constant secular rate: $\dot{\varpi}_\pm = B(2-\sigma)/2 \mp \omega_T$.

When $\sigma = 0$ is set while $I_{xx} = I_{yy} \le I_{zz}$ is kept, these averaged equations will reduce to the classical equations describing the averaged orbit elements about a body with J_2 (Ref. 3). Thus, we see that the effect of the body's equatorial ellipticity is to cause a nutation in the orbit plane, that is, a change in inclination, in addition to the precession of the orbit plane that is already present for the $\sigma = 0$ case.

D. Averaging the Jacobi Integral

Because the Jacobi integral is a constant, it can be averaged over to yield the same value. Note, however, that averaging the functional side of the integral does introduce some subtle, but important, changes. Performing the averaging on the integral yields

$$\bar{J} = -\mu/(2a) - \omega_T\sqrt{\mu a(1-e^2)}\cos i - \bar{U}_{20+22} \tag{28}$$

where the orbital elements on the right-hand side are interpreted as mean elements. From Eqs. (20) and (21) we note that the semimajor axis a and eccentricity e are conserved on average and can be removed to define a new, simplified form of the constant:

$$C = \left(1 - \sigma\cos^2\Omega_R\right)\sin^2 i - (2\omega_T/B)\cos i \tag{29}$$

The quantity in Eq. (29) is conserved among the mean orbital elements only and not among the unaveraged osculating elements.

IV. Analysis

By using both the averaged Jacobi integral and the averaged Lagrange equations, we can reduce this problem to quadratures and find a complete qualitative understanding of orbital motion for this problem.

A. Reduction to Quadratures

Note that Eqs. (22), (23), and (29) only contain the two averaged orbital elements Ω_R and i. Thus, we can use Eq. (29) to reduce either of Eqs. (22) or (23) into a form that can be reduced to quadratures. Applying this reduction to both equations yields

$$\frac{\mathrm{d}i}{\mathrm{d}t} = \frac{B}{\sin i}\sqrt{\left[(\sigma-1)\sin^2 i + C + (2\omega_T/B)\cos i\right]\left[\sin^2 i - C - (2\omega_T/B)\cos i\right]} \tag{30}$$

$$\frac{\mathrm{d}\Omega_R}{\mathrm{d}t} = -\frac{B}{2}\left[2\omega_T/B \pm \sqrt{(2\omega_T/B)^2 + 4\left(1 - C - \sigma\cos^2\Omega_R\right)\left(1 - \sigma\cos^2\Omega_R\right)}\right] \tag{31}$$

We note that either of these equations can be reduced to a quadrature of the form

$$t - t_0 = \int_{i_0}^{i} \frac{1}{g(i)}\,\mathrm{d}i \tag{32}$$

$$t - t_0 = \int_{\Omega_{R0}}^{\Omega_R} \frac{1}{f(\Omega_R)}\,\mathrm{d}\Omega_R \tag{33}$$

Subsequent to evaluating these integrals, Eqs. (24) and (25) can also be reduced to a quadrature. This indicates that the averaged problem is completely integrable. The special case of $\omega_T = 0$ was considered,[2] and the quadrature indicated in Eq. (33) was carried out explicitly, yielding closed-form solutions for the mean orbital elements in terms of elliptic functions and integrals.

B. Jacobi Contours

Even though the averaged orbit dynamics can be reduced to quadratures, this does not give us any direct insight into how the orbit will evolve. Such insight can be obtained, however, by plotting Eq. (29) along contours of constant C as a function of i and Ω_R. In Figs. 3–6 we show a sequence of contours for a generic situation with $\sigma \in (0, 1)$ for values of ω_T increasing from zero. In Figs. 3–6, the inclination i and relative node Ω_R will follow along the curves of constant contour.

Figure 3 recreates a figure for the case $\omega_T = 0$ (Ref. 2). Here, we note that there are two fundamental types of motion possible for the inclination and longitude of the ascending node (in the body-fixed frame). The orbit plane will either be in circulation, corresponding to a secularly changing Ω_R, or in libration, corresponding to the inclination oscillating about 90 deg and the node oscillating about ± 90 deg. We note four points at which the inclination and node will remain stationary: $i = 90$ deg and $\Omega_R = 0, \pm 90$, and 180 deg. From the contours, it is evident that two of these solutions ($\Omega_R = \pm 90$ deg) are stable and two ($\Omega_R = 0$ and 180 deg) are unstable. Note that, even though i and Ω_R can have stationary values in the body-fixed frame, the argument of periapsis will not be stationary in general but will instead have a constant secular increase when at these points.

In Figs. 4–6, we show the Jacobi contours when $\omega_T > 0$. We note that the zones of libration are pushed to higher inclinations. As ω_T increases the unstable point eventually disappears when it is pushed into a retrograde, equatorial orbit. As ω_T is increased further, the stable point also disappears in the same fashion. For rotation rates larger than this the orbit plane will always have a secular precession in the body-fixed frame. In Fig. 5, we note that the separation line between circulation and libration terminates in the line of equatorial, retrograde orbits ($i = 180$ deg). The separation line acts as a heteroclinic orbit connecting these equatorial, retrograde orbits to themselves, although the orbital dynamics in the equator have a fundamental separation from motion out of the equator. This separatrix exists for rotation rates between the two critical values where the unstable and stable equilibrium points disappear.

C. Partially Frozen Orbits

A frozen orbit is generally defined as an orbit with no secular motion, or as an equilibrium point to the averaged Lagrange planetary equations. In this problem we do not find completely frozen orbits, in general, because the argument of periapsis usually has a nonzero secular increase. We do find, however, families of orbits where the orbital plane of the spacecraft is frozen in the body-fixed frame, corresponding to stationary values for the inclination i and longitude of the ascending node Ω_R. These points are clearly seen in the Jacobi contours and can be explicitly found from the Lagrange equations as well. We will look at the unstable and stable points separately.

1. *Unstable Orbit*

Setting $\Omega_R = 0$ or 180 deg, we see from Eqs. (22) and (23) that

$$\frac{\mathrm{d}i_0}{\mathrm{d}t} = 0 \tag{34}$$

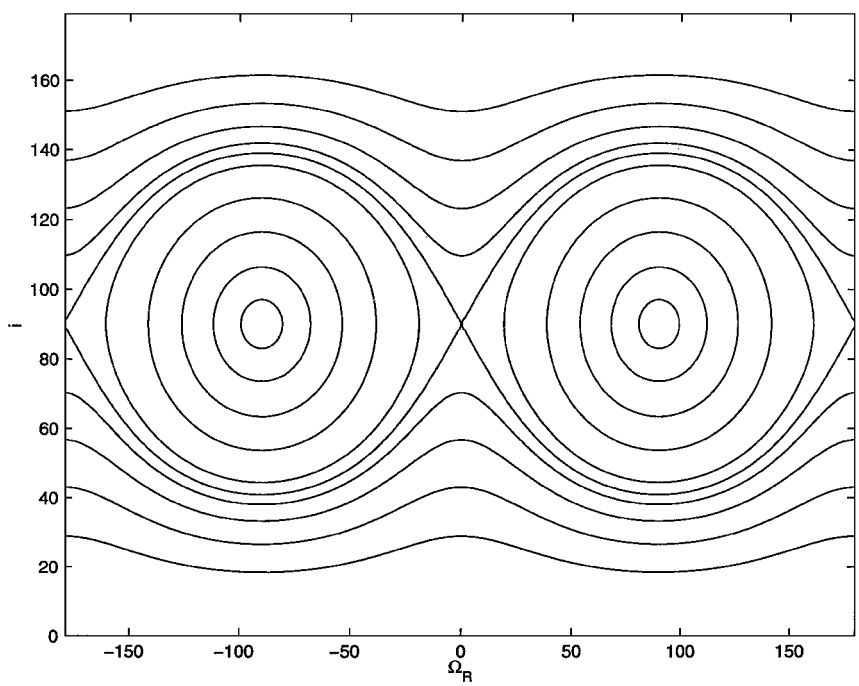

Fig. 3 Contour plots of Eq. (29) as a function of inclination i and node Ω_R for the case of no rotation ($\omega_T = 0$).

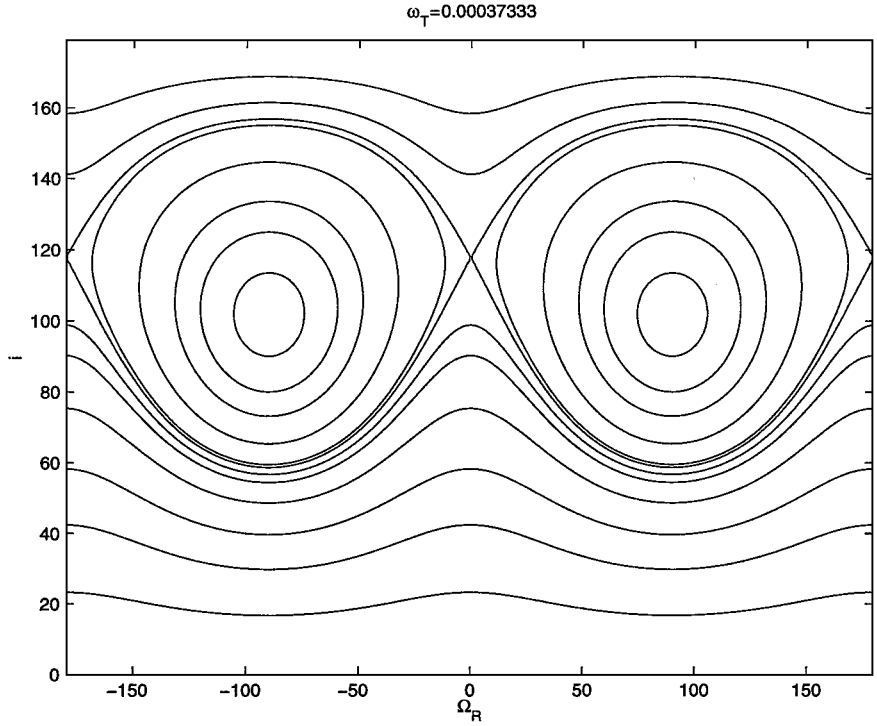

Fig. 4 Contour plots of Eq. (29) as a function of inclination i and node Ω_R for the case of slow rotation.

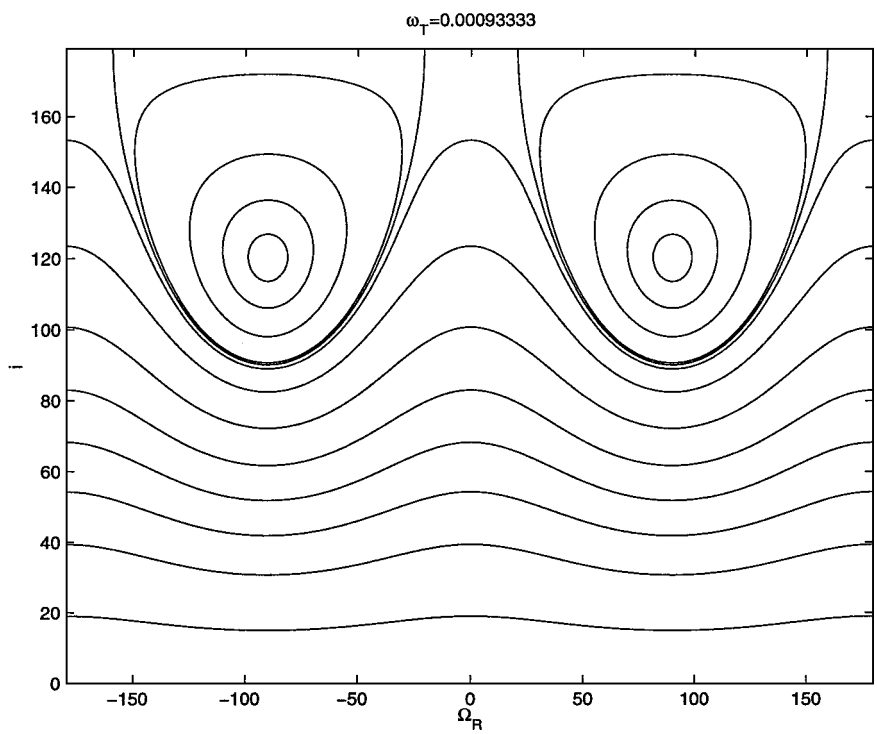

Fig. 5 Contour plots of Eq. (29) as a function of inclination i and node Ω_R for the case $\omega_{T_u} < \omega_T < \omega_{T_s}$.

$$\frac{\mathrm{d}\Omega_{R0}}{\mathrm{d}t} = -B(1-\sigma)\cos i_0 - \omega_T \tag{35}$$

Thus, we derive a simple condition on inclination for the relative node to be frozen:

$$\cos i_0 = -\omega_T/[B(1-\sigma)] \tag{36}$$

A simple analysis of this solution shows that it is unstable. We assume $\Delta\Omega_R = \Omega_R - \Omega_{R0}$ and $\Delta i = i - i_0$ at these frozen points. The local linearized equations are

$$\frac{\mathrm{d}\Delta i}{\mathrm{d}t} = B\sigma \sin i_0 \Delta\Omega_R \tag{37}$$

$$\frac{\mathrm{d}\Delta\Omega_R}{\mathrm{d}t} = B(1-\sigma)^2 \sin i_0 \Delta i \tag{38}$$

Their characteristic equation is $\lambda^2 - B^2\sigma(1-\sigma)^2 \sin^2 i_0 = 0$. Hence, the equilibrium is a saddle point. The argument of periapsis will have a constant secular rate at this point equal to

$$\frac{\mathrm{d}\omega}{\mathrm{d}t} = -\frac{B}{2}(1-2\sigma) + \frac{5}{2}\frac{\omega_T^2}{B(1-\sigma)} \tag{39}$$

Thus, as ω_T is increased from zero, the inclination of the frozen orbit in Eq. (36) is pushed to higher values. When the inclination is pushed to 180 deg, the equation for the relative node is no longer

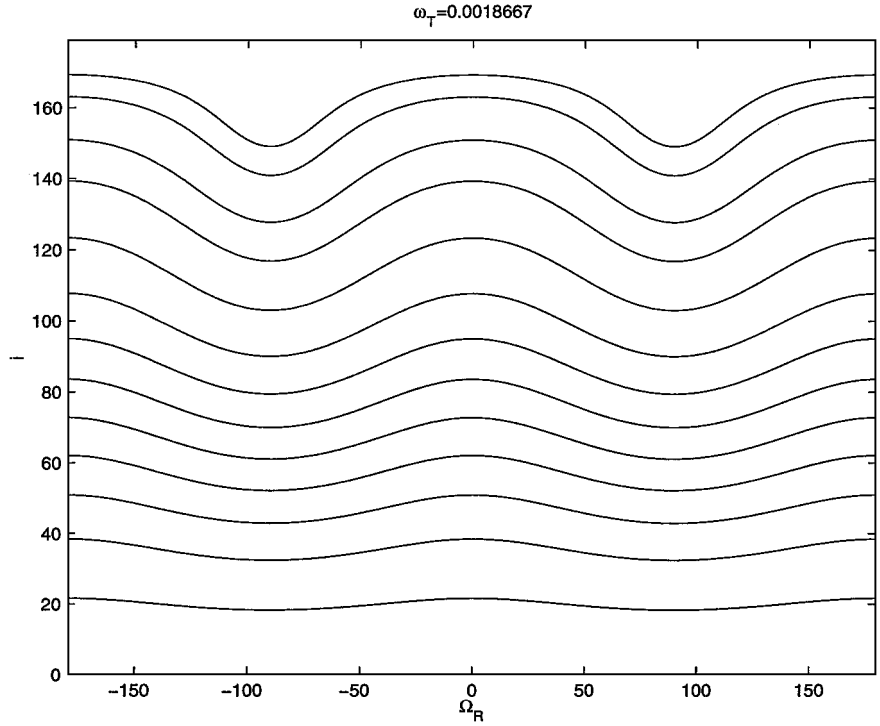

Fig. 6 Contour plots of Eq. (29) as a function of inclination i and node Ω_R for the case $\omega_T > \omega_{T_s}$.

defined, and the frozen orbit disappears. (Note that the longitude of periapsis for an equatorial, retrograde orbit has a constant secular rate.) The critical value of the asteroid rotation rate when the unstable equilibrium point disappears is

$$\omega_{T_u} = (1-\sigma)B \tag{40}$$

or, in terms of the orbit period of the spacecraft,

$$T_u = T_{S/C}\frac{2a^2(1-e^2)^2}{3(I_{zz}-I_{xx})(1-\sigma)} = T_{S/C}\frac{2p^2}{3(I_{zz}-I_{yy})} \tag{41}$$

Thus, we see that the critical rotation period depends on the spacecraft orbit period, orbit parameter, and the shape of the rotating asteroid.

For asteroid rotation rates greater than ω_{T_u}, we can still use Eq. (23) to delineate where the line between circulation and libration of the orbit plane occurs. This is done by artificially treating Eq. (23) as an equilibrium point for the case $i = 180$ deg, yielding an explicit solution for the relative node:

$$\cos^2\Omega_R = (B-\omega_T)/(\sigma B) \tag{42}$$

We see that $\cos^2\Omega_R = 1$ at the critical rotation rate $\omega_{T_u} = B(1-\sigma)$ and that $\cos^2\Omega_R = 0$ when the rotation rate is increased to a value equal to B. In the next subsection, we shall see that this corresponds to the disappearance of the stable frozen orbit. The value of Ω_R computed from this relation will then predict the intersection point of the separatrix between circulation and libration with $i = 180$ deg.

2. Stable Orbit

Next, with the setting $\Omega_R = \pm 90$ deg, Eqs. (22) and (23) reduce to

$$\frac{\mathrm{d}i_0}{\mathrm{d}t} = 0 \tag{43}$$

$$\frac{\mathrm{d}\Omega_{R0}}{\mathrm{d}t} = -B\cos i_0 - \omega_T \tag{44}$$

Thus, the condition to freeze the relative node reduces to the condition on inclination

$$\cos i_0 = -\omega_T/B \tag{45}$$

Again, by assuming $\Delta\Omega_R = \Omega_R - \Omega_{R0}$ and $\Delta i = i - i_0$ at these frozen points, we have the local linearized equations

$$\frac{\mathrm{d}\Delta i}{\mathrm{d}t} = -B\sigma\sin i_0\Delta\Omega_R \tag{46}$$

$$\frac{\mathrm{d}\Delta\Omega_R}{\mathrm{d}t} = B(1-\sigma)\sin i_0\Delta i \tag{47}$$

Their characteristic equation is $\lambda^2 + B^2\sigma(1-\sigma)\sin^2 i_0 = 0$. Thus, the equilibrium is a center. The argument of periapsis will have a constant secular rate at this point equal to

$$\frac{\mathrm{d}\omega}{\mathrm{d}t} = -\frac{B}{2}(1+\sigma) + \frac{5}{2}\frac{\omega_T^2}{B} \tag{48}$$

As ω_T is increased from zero, the inclination in Eq. (45) is pushed from 90 deg to higher values. The critical rotation period, where the stable orbit ceases to exist, now occurs when

$$\omega_{T_s} = B \tag{49}$$

or in terms of the orbit period of the spacecraft as

$$T_s = T_{S/C}\frac{2p^2}{3(I_{zz}-I_{xx})} = T_u(1-\sigma) \tag{50}$$

For asteroids rotating at a faster rate (with a shorter period), we see that the orbit plane can only be in circulation, albeit with a predictable nutation amplitude as a function of inclination.

3. Direct and Retrograde Orbit

In the two preceding sections, we briefly discussed the stability of the direct orbit when $i = 0$ deg and the retrograde orbit when $i = 180$ deg. Strictly speaking, there is no definition of Ω_R for these two cases. Let us use new variables p_1 and q_1 instead of the traditional i and Ω_R to study the stability of these two special orbits. From the definition of inclination and ascending node, $i = 0$ and $\omega_T < 0$ is equivalent to $i = 180$ deg and $\omega_T > 0$, so that we can just study direct orbits and include retrograde orbits by considering the case $\omega_T < 0$, $i = 0$ deg. Let

$$p_1 = \tan(i/2)\sin\Omega_R \tag{51}$$

$$q_1 = \tan(i/2)\cos\Omega_R \tag{52}$$

The secular rate of p_1 and q_1 can be found by using the averaged equations (22) and (23):

$$\frac{\mathrm{d}p_1}{\mathrm{d}t} = \frac{Bq_1}{1+p_1^2+q_1^2}\left[\sigma\left(1+p_1^2-q_1^2\right)-\left(1-p_1^2-q_1^2\right)\right]-\omega_T q_1 \tag{53}$$

$$\frac{\mathrm{d}q_1}{\mathrm{d}t} = \frac{Bp_1}{1+p_1^2+q_1^2}\left[2\sigma q_1^2+\left(1-p_1^2-q_1^2\right)\right]+\omega_T p_1 \tag{54}$$

The equilibrium point of the preceding equation is $p_{10}=q_{10}=0$ when $i=0$ deg. By linearization using $\Delta p_1 = p_1 - p_{10}$ and $\Delta q_1 = q_1 - q_{10}$, we have

$$\frac{\mathrm{d}\Delta p_1}{\mathrm{d}t} = -[B(1-\sigma)+\omega_T]\Delta q_1 \tag{55}$$

$$\frac{\mathrm{d}\Delta q_1}{\mathrm{d}t} = (B+\omega_T)\Delta p_1 \tag{56}$$

The stability condition on this equation is

$$[B(1-\sigma)+\omega_T](B+\omega_T) > 0 \tag{57}$$

Because $B>0$ and $\sigma<1$, Eq. (57) implies that the direct orbit for $i=0$ and $\omega_T>0$ is always stable independent of the central body rotation rate ω_T, whereas the retrograde orbit for $i=0$ and $\omega_T<0$ is stable only when $|\omega_T|<B(1-\sigma)$ or $|\omega_T|>B$ and is unstable in the interval $B(1-\sigma)<|\omega_T|<B$. The unstable situation occurs when the stable frozen orbit exists and the unstable frozen orbit disappears, that is, $\omega_{Tu}<|\omega_T|<\omega_{Ts}$. The instablity region for the retrograde orbit is

$$\Delta\omega_{Tu} = \omega_{Ts}-\omega_{Tu} = \sigma B = \frac{3\mu^{\frac{1}{2}}(I_{zz}-I_{xx})\sigma}{2a^{\frac{7}{2}}(1-e^2)^2} = \frac{3n(I_{yy}-I_{xx})}{2p^2} \tag{58}$$

This indicates that a retrograde orbit in this situation is susceptible to an out-of-plane instability. Thus, the results here correspond to the unstable and stable orbits analyses in the two preceding sections.

The stability condition for the retrograde orbit can also be obtained by following the preceding analysis procedure but instead defining $p_2 = \cot(i/2)\sin\Omega_R$, $q_2 = \cot(i/2)\cos\Omega_R$, and $\omega_T>0$.

D. Similarity to the Free Rigid-Body Motion

The orbital angular momentum unit vector components in rotating coordinates are

$$h_x = \sin i \sin\Omega_R \tag{59}$$

$$h_y = -\sin i\cos\Omega_R \tag{60}$$

$$h_z = \cos i \tag{61}$$

The averaged dynamics of the momentum can be found by using Eqs. (22) and (23):

$$\frac{\mathrm{d}h_x}{\mathrm{d}t} = [B(1-\sigma)h_z+\omega_T]h_y \tag{62}$$

$$\frac{\mathrm{d}h_y}{\mathrm{d}t} = -(Bh_z+\omega_T)h_x \tag{63}$$

$$\frac{\mathrm{d}h_z}{\mathrm{d}t} = B\sigma h_x h_y \tag{64}$$

There are six equilibrium points (as will be shown later) that correspond to the two unstable frozen orbits, the two stable frozen orbits, the direct orbit, and the retrograde orbit that were discussed in the preceding sections. The averaged angular momentum dynamics are quite similar to the free rigid-body motion, especially when $\omega_T=0$. This is why there are several phenomena in our problem that are quite similar to the torque-free rigid-body motion. For example, consider a particle's orbit plane precessing around a principal axis of inertia I_1 of the central body. Its secular orbit stability condition is then similar to the stability condition of a torque-free rigid-body motion. The equivalent stability condition to Eq. (57) is

$$\left[(3n/2p^2)(I_1-I_2)+\omega_T\right]\left[(3n/2p^2)(I_1-I_3)+\omega_T\right] > 0 \tag{65}$$

where I_1 is the central body rotation axis and I_2 and I_3 are the other two principal axes of inertia. It can be seen that there are some similarities between the stability conditions of the torque-free rigid-body rotational motion and our problem of a particle moving around a rigid body, especially when $\omega_T=0$. For rigid-body motion, rotation is stable when the rigid body rotates about its largest or smallest moment of inertia. For our problem, the particle's motion is also stable when it circles the axis of the largest or smallest moment of inertia of the central body. There are some fundamental reasons for this similarity because the two kinds of motions are both determined by the mass distribution of the central body that is described by the moments of inertia. This similarity can give us insight into stable and unstable orbits in the second-degree and second-order gravity field.

E. Dimensionless Analysis and Application

To give a more physically motivated example for our discussion, we assume that the second-degree and second-order gravity coefficients are derived from a constant density, triaxial ellipsoid shape. This assumption is not necessary, but provides a physical realization of our system. Assume a central body with semi-axes of $\alpha\geq\beta\geq\gamma$. According to our coordinate frame definitions, α is along the x axis, whereas β is measured along the y axis, and γ is measured along the z axis (see Fig. 1). Instead of using the semimajor axes β and γ, we can also use the ellipticities of the ellipsoid

$$\beta = \alpha\sqrt{1-\epsilon_b^2} \tag{66}$$

$$\gamma = \alpha\sqrt{1-\epsilon_c^2} \tag{67}$$

Thus, with our ordering convention, we have $\epsilon_b\leq\epsilon_c$ and $\sigma=\epsilon_b^2/\epsilon_c^2$. When the ellipsoid eccentricities go to zero, the body goes to a sphere, whereas as they go to 1, the body approaches a slender rod. With these definitions, the gravity coefficients can be rewritten as

$$C_{20} = -\tfrac{1}{10}(\alpha^2+\beta^2-2\gamma^2) \tag{68}$$

$$= -\left(\alpha^2\epsilon_c^2/10\right)(2-\sigma) \tag{69}$$

$$C_{22} = \tfrac{1}{20}(\alpha^2-\beta^2) = \left(\alpha^2\epsilon_c^2/20\right)\sigma \tag{70}$$

If we use $\mathrm{d}\theta=\omega_T\,\mathrm{d}t$ instead of $\mathrm{d}t$ in Eqs. (20–25), the averaged equations become dimensionless, and the constant B becomes

$$\tilde{B} = \frac{B}{\omega_T} = \frac{3\mu^{\frac{1}{2}}(I_{zz}-I_{xx})}{2a^{\frac{7}{2}}(1-e^2)^2\omega_T} \tag{71}$$

$$= \frac{3\mu^{\frac{1}{2}}}{a^{\frac{7}{2}}(1-e^2)^2\omega_T}\left(\frac{\alpha^2\epsilon_c^2}{10}\right) \tag{72}$$

$$= \frac{\sqrt{3\rho G}\left(1-\epsilon_b^2\right)^{\frac{1}{4}}\left(1-\epsilon_c^2\right)^{\frac{1}{4}}\epsilon_c^2\alpha^{\frac{7}{2}}}{5\omega_T(1-e^2)^2a^{\frac{7}{2}}} \tag{73}$$

where $\mu=(\frac{4}{3})\pi\alpha\beta\gamma\rho G$, ρ is the density of the ellipsoid, and G is the gravity constant. $\tilde{B}$ is a dimensionless parameter that, in addition with σ, characterizes the averaged orbital motion of the particle in the second-degree and second-order gravity field.

Now the retrograde orbit ($i = 180$ deg and $\omega_T > 0$) is unstable, when $1 < \tilde{B} < 1/(1-\sigma)$. The values of 1 and $1/(1-\sigma)$ of $\tilde{B}$ are also the critical conditions for the existence of the stable and the unstable frozen orbits, respectively [see Eqs. (40) and (49)]. When $\tilde{B} > 1$, the stable 1:1 orbit exists, and when $\tilde{B} > 1/(1-\sigma)$, the unstable 1:1 orbit exists. It can be seen that the value of $\tilde{B}$ is related with both the parameters of the central body and the spacecraft orbit. If we define the minimum circular orbit as the orbit when $a = \alpha$ and $e = 0$, a new parameter can be found that is determined only by the central body's density, shape, and rotation rate:

$$\tilde{B}^* = \sqrt{3\rho G}\left(1-\epsilon_b^2\right)^{\frac{1}{4}}\left(1-\epsilon_c^2\right)^{\frac{1}{4}}\epsilon_c^2 \Big/ (5\omega_T) \tag{74}$$

When $\tilde{B}^* > 1$, the stable 1:1 circular orbit can physically exist, and when $\tilde{B}^* > 1/(1-\sigma)$, the unstable 1:1 orbit physically exists (because $a > \alpha$, in general). Thus, the variable $\tilde{B}^*$ can be used to check if the resonant 1:1 orbits can exist for a particular asteroid that, in turn, will be a measure of how important the effects described here will be for any given asteroid.

The condition $\tilde{B}^* > 1$ can be restated as a condition on the density and rotation period of the asteroid that can be combined into one variable. When

$$\sqrt{\rho T^2} > 10\pi \Big/ \left[\sqrt{3G}\left(1-\sigma\epsilon_c^2\right)^{\frac{1}{4}}\left(1-\epsilon_c^2\right)^{\frac{1}{4}}\epsilon_c^2\right] \tag{75}$$

the minimum circular orbit exists, and the effects described in this paper are important. The right-hand side of the preceding inequality is determined only by the shape of the asteroid, which can be estimated from ground-based observation of the asteroid. The minimum value of the right-hand side occurs when

$$\epsilon_c^2 = \left[5(1+\sigma) - \sqrt{25\sigma^2 - 46\sigma + 25}\right] \Big/ (12\sigma) \tag{76}$$

For example, when $\sigma = 1$, the minimum point is $\epsilon_c^2 = \frac{2}{3}$ and leads to $\sqrt{(\rho T^2)} > 50.7$ (g/cm^3)$^{1/2}$ h. Figure 7 shows the curves of Eq. (75) for different values of σ. The overall pattern of the curves is similar.

The rotation rate and size of 748 asteroids have been analyzed,[13] with about 10% of the asteroids being slow rotators for which the spin period is more than 20 h. One of the largest known slow rotators is (253) Mathilde with diameter $D = 58$ km, $T = 418$ h, and density $\rho = 1.3$ g/cm^3. We can see that the slow rotation effects will play an important role in spacecraft motion about this body as $T \gg 50.7/\sqrt{\rho} = 44.7$ h when $\sigma = 1$ and $\epsilon_c^2 = \frac{2}{3}$.

Finally, we make a cursory check of our assumptions in performing the averaging of the potential. In terms of the period of the spacecraft orbit relative to the rotation period of the asteroid, we had assumed that $T_{S/C} \ll T$, which corresponds to the inequality

$$\frac{T_{S/C}}{T} = \frac{3(I_{zz} - I_{yy})}{2p^2} = \frac{3}{10}\left(\frac{\alpha}{p}\right)^2 \epsilon_c^2(1-\sigma) \ll 1 \tag{77}$$

By inspection, we note that each of the terms in the equation is less than one, and, hence, their product will be less than one.

F. Discussion

The results in this section give a global, qualitative description of orbital motion. The main result applies to the motion of the orbit plane because it exhibits two very different modes as a function of initial conditions and parameters. In the librational mode, the precession rate of the orbit plane is in a 1:1 resonance with the asteroid rotation rate. Thus, in the body-fixed frame, the orbit normal is seen to librate about a fixed direction in this frame. Physically, the asteroid gravity field is dragging the orbit plane along with itself, something that can only occur for a slow enough asteroid rotation rate. A similar phenomenon was observed for orbital motion about the slowly tumbling asteroid Toutatis.[16]

When the orbit plane is in circulation mode its precession rate is not equal to the asteroid rotation rate. Thus, on average, the longitude of the ascending node will circulate around the asteroid. We see that there can still be significant nutation of the orbit plane in this case, although the nutation amplitude decreases as the magnitude of the body-relative precession rate increases.

We can also relate the orbit plane motion in the body-fixed frame to orbit plane precession in the inertially fixed frame. Here, we note that $\dot{\Omega} = \dot{\Omega}_R + \omega_T = -B\cos i(1 - \sigma\cos^2\Omega_R)$. Thus, we still have the result that the precession rate of the orbit plane is zero at an inclination of 90 deg, but now, due to the nutation of the orbit plane, the orbit inclination will not remain fixed at 90 deg and will instead oscillate about this value.

V. Numerical Calculations and Verifications

To complete this study we present a number of numerical integrations that give partial validation of the assumptions made and

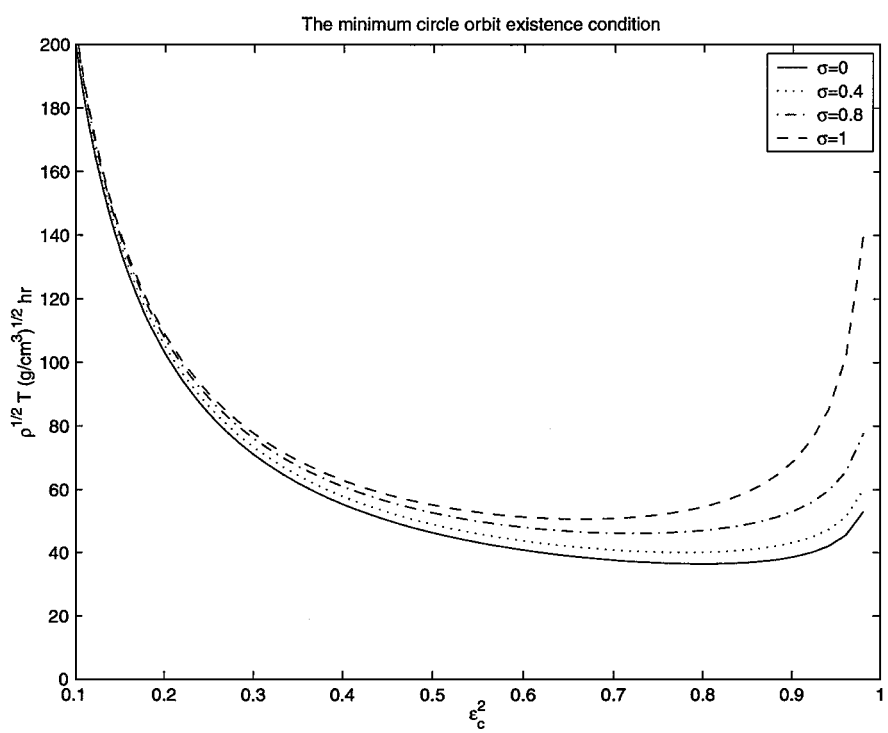

Fig. 7 Plots of Eq. (75) for different values of σ; note that the minimum $\sqrt{\rho T}$ exists and is a function of ϵ_c^2.

that verify that the predicted behavior of the orbit plane does indeed occur. Because of the nature of numerical computations we can, realistically, only check our assumptions at a few points, but agreement for a generically chosen set of conditions in the interval under consideration will give us confidence in the analysis on the whole. The numerical approach solves Eqs. (12–14) by direct numerical integration of accelerations and velocities in the body-fixed space. The osculating orbital elements are computed at each time step by transforming the position and velocity vectors from the body-fixed state to inertial coordinates.

First consider Fig. 8, which shows the osculating orbit elements from a particular numerical solution when $\omega_T = 3.733 \times 10^{-4}$ and $\sigma = \frac{4}{7}$. From this, we clearly see that the orbital elements a and e are constant on average as predicted from our averaging analysis. We see that the other elements have nontrivial motions and that the Jacobi integral is constant.

Next consider Fig. 9, which compares a single orbit of Ω_R vs i, as computed from the analytical theory[2] for $\omega_T = 0$, with a numerical integration of a similar orbit, the two curves superimposed. This case represents a solution where the orbit plane has a nutation amplitude of ± 45 deg about a polar orbit and has a precession of the same amplitude about $\Omega_R = 90$ deg. We see close agreement between the averaged and numerical solutions, clearly indicating that our averaged analysis captures the essential character of motion in this case.

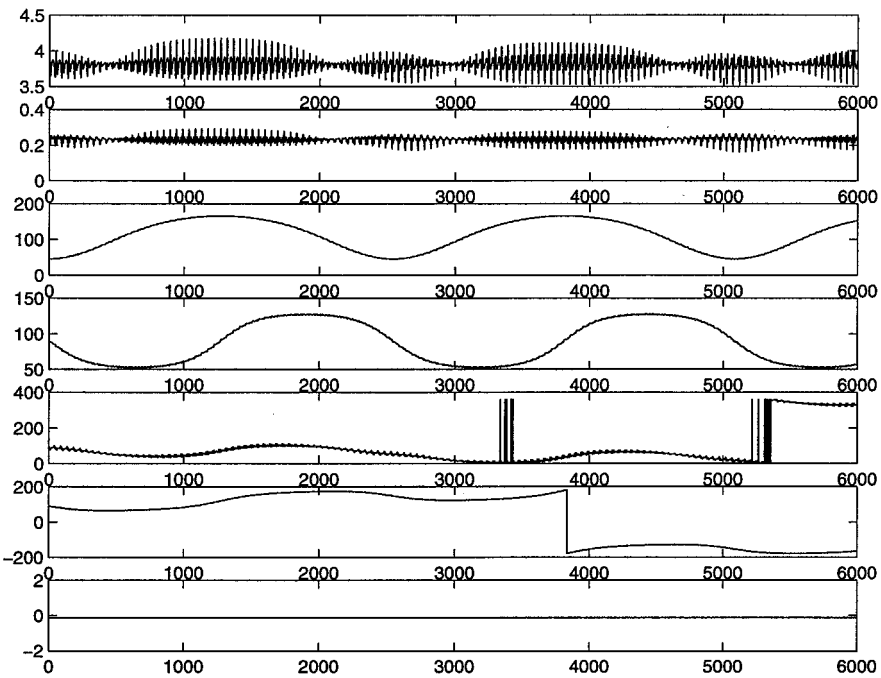

Fig. 8 Numerically computed osculating orbital elements and Jacobi constant for a generic orbit; shown in order from top to bottom are a, e, i, Ω_R, ω, Ω, and J.

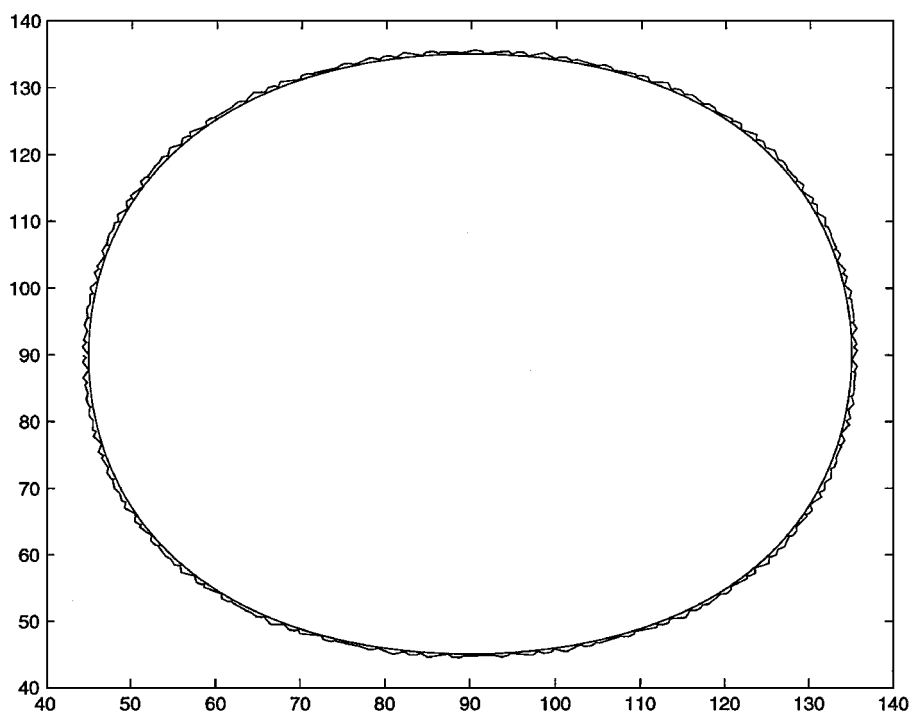

Fig. 9 Quantitative comparison of the averaged analytical solution[2] for i and Ω_R and the numerical solution of these quantities for $\omega_T = 0$.

Finally, consider Fig. 10, which shows the results of a number of numerical integrations plotted in the Ω_R–i space when $\mu = 1.0$, $\omega_T = 3.733 \times 10^{-4}$, and $\sigma = \frac{4}{7}$ ($C_{20} = -0.1$ and $C_{22} = 0.02$). We note that this computation recreates the curves from our averaged analysis. Again, for this particular case, we see that the contours generated are qualitatively equivalent to those generated from the averaged theory. Note that the contour lines in Figs. 3–6 are not lines of constant Jacobi integral values in the unaveraged problem. This result validates our approach and shows that we can project the five-dimensional surface of constant Jacobi values onto a two-dimensional space and reduce the general problem of orbiting about a slowly rotating, second-degree, and second-order gravity field to a series of contour plots showing how the orbit plane precesses and nutates.

Figure 11 shows the orbit angular momentum vector in three-dimensional space, corresponding to Fig. 10. We note that this

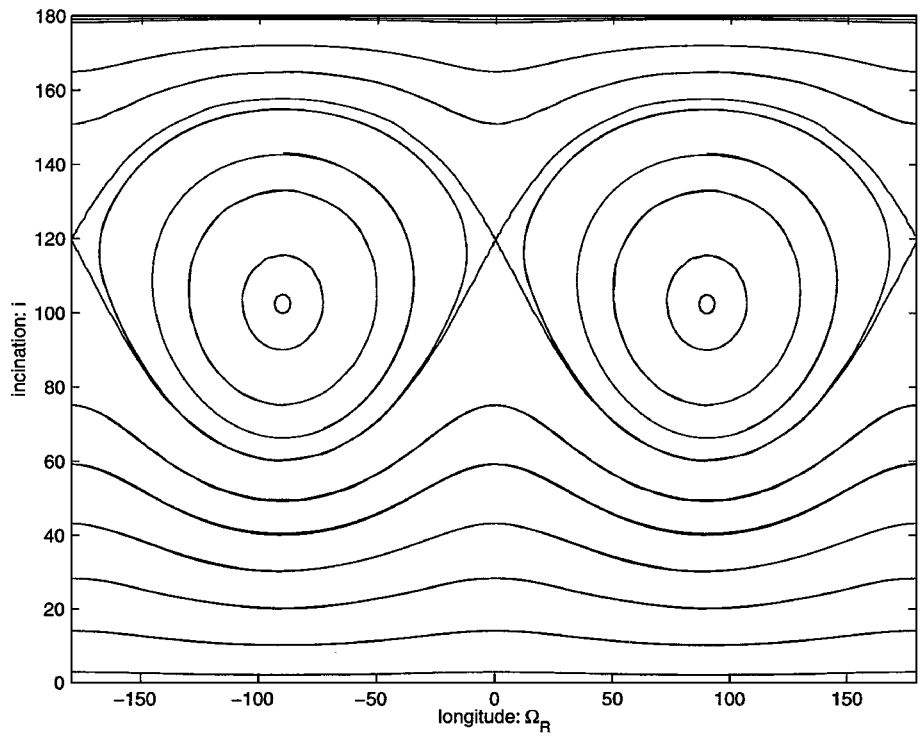

Fig. 10 Numerical calculation of the contours of Ω_R and i for a range of different initial conditions.

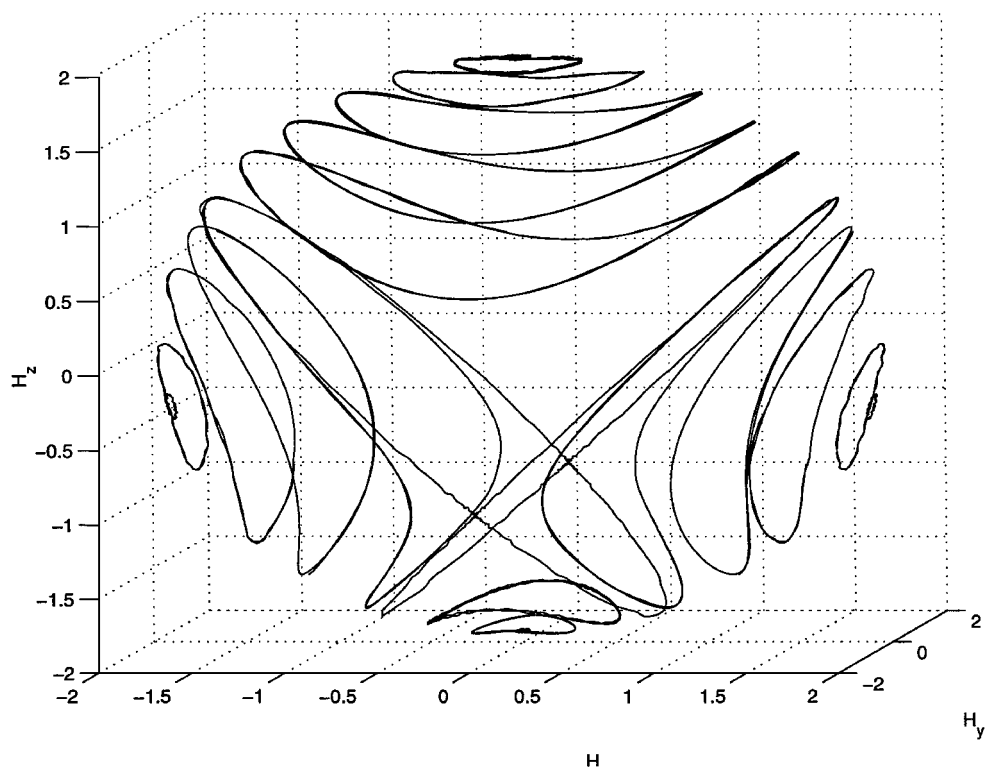

Fig. 11 Numerical calculation of the angular momentum vector in three-dimensional space for a range of different initial conditions.

computation uses the same initial conditions for Fig. 10. We see that the averaged equations (62–64) completely describe the orbital angular momentum motion.

Particularly interesting are the separatrices between the libration and circulation cases, heteroclinic connections between the unstable frozen orbits for the mean elements in our averaged motion analysis. The orbit normal can cross these lines without violating any fundamental uniqueness properties of the full solution. Thus, it is possible for orbital motion in the real system to jump between circulation and libration, potentially defining a region of chaotic motion in terms of the orientation of the orbit plane.

VI. Conclusions

The case of spacecraft motion about an arbitrary second-degree and second-order gravity field is studied for the case in which the central body is slowly rotating. This problem is directly applicable to orbital motion about asteroids. The averaged problem of orbital motion is defined and shown to be integrable in the formal sense. By proper application of the Jacobi integral, we are able to describe completely the secular motion of the spacecraft orbit plane. For a slowly rotating asteroid, it is possible for the orbit plane to become captured by the rotating body, leading to a librational motion of the orbit plane in the body-fixed space. For faster rotation values, the asteroid can no longer capture the orbit plane in such a manner.

Acknowledgment

The work described was funded by the Telecommunications and Mission Operations Directorate Technology Program with a grant from the Jet Propulsion Laboratory, California Institute of Technology, which is under contract with NASA.

References

[1]Scheeres, D. J., "Dynamics About Uniformly Rotating TriAxial Ellipsoids: Applications to Asteroids," *Icarus*, Vol. 110, No. 1, 1994, pp. 225–238.

[2]Scheeres, D. J., and Hu, W., "Secular Motion in a 2nd Degree and Order Gravity Field with No Rotation," *Celestial Mechanics and Dynamical Astronomy*, Vol. 79, No. 3, 2001, pp. 173–200.

[3]Garfinkel, B., "On the Motion of a Satellite of an Oblate Planet," *Astronomical Journal*, Vol. 63, No. 1257, 1958, pp. 88–96.

[4]Kozai, Y., "The Motion of a Close Earth Satellite," *Astronomical Journal*, Vol. 64, No. 1274, 1959, pp. 367–377.

[5]Brouwer, D., "Solution of the Problem of Artificial Satellite Theory Without Drag," *Astronomical Journal*, Vol. 64, No. 1274, 1959, pp. 378–397.

[6]Brouwer, D., and Clemence, G. M., *Methods of Celestial Mechanics,* Academic Press, New York, 1961, p. 290.

[7]Kaula, W. M., *Theory of Satellite Geodesy,* Blaisdell, Boston, 1966, pp. 49–56.

[8]Gedeon, G. S., "Tesseral Resonance Effects on Satellite Orbits," *Celestial Mechanics and Dynamical Astronomy*, Vol. 1, 1969, pp. 167–189.

[9]Ely, T. A., and Howell, K. C., "Long-Term Evolution of Artificial Satellite Orbits due to Resonant Tesseral Harmonics," *Journal of the Astronomical Science*, Vol. 44, No. 2, 1996, pp. 167–190.

[10]Scheeres, D. J., "The Effect of C_{22} on Orbit Energy and Angular Momentum," *Celestial Mechanics and Dynamical Astronomy*, Vol. 73, No. 1/4, 1999, pp. 339–348.

[11]Scheeres, D. J., Williams, B. G., and Miller, J. K., "Evaluation of the Dynamic Environment of an Asteroid: Applications to 433 Eros," *Journal of Guidance, Control, and Dynamics*, Vol. 23, No. 3, 2000, pp. 466–475.

[12]Kozai, Y., "Secular Perturbation of Asteroids with High Inclination and Eccentricity," *Astronomical Journal*, Vol. 67, No. 9, 1962, pp. 591–598.

[13]Pravec, P., and Harris, A. W., "Fast and Slowly Rotating Asteroids," *Icarus*, Vol. 148, No. 1, 2000, pp. 12–20.

[14]Harris, A. W., "Tumbling Asteroids," *Icarus*, Vol. 107, No. 1, 1994, pp. 209–211.

[15]Hudson, R. S., and Ostro, S. J., "Shape and Non-Principal Axis Spin State of Asteroid 4179 Toutatis," *Science*, Vol. 270, No. 5233, 1995, pp. 84–86.

[16]Scheeres, D. J., Ostro, S. J., Hudson, R. S., DeJong, E. M., and Suzuki, S., "Dynamics of Orbits Close to Asteroid 4179 Toutatis," *Icarus*, Vol. 132, No. 1, 1998, pp. 53–79.